TIME-OF-FLIGHT HE+ BEAM POTENTIAL DIAGNOSTIC IN TANDEM MIRRORS

by

B. T. Archer and M. A. Lieberman

Memorandum No. UCB/ERL M85/34

29 April 1985

Cover Page

TIME-OF-FLIGHT HE+ BEAM POTENTIAL DIAGNOSTIC IN TANDEM MIRRORS

by

B. T. Archer and M. A. Lieberman

Memorandum No. UCB/ERL M85/34

26 April 1985

ELECTRONICS RESEARCH LABORATORY

College of Engineering
University of California, Berkeley
94720

Time-of-flight He^+ Beam Potential Diagnostic in Tandem Mirrors

B. T. Archer and M. A. Lieberman

April 15, 1985

ELECTRONICS RESEARCH LABORATORY
College of Engineering
University of California, Berkeley, CA 94720

This work was supported by DOE Contract No. DE-AT03-76ET53059.

Time-of-flight He^+ Beam Potential Diagnostic in Tandem Mirrors

B. T. Archer and M. A. Lieberman

The feasibility of a modulated He^+ beam as an electrostatic potential diagnostic in tandem mirrors is investigated. The modulated beam is injected axially along the central magnetic field line of the machine. Collisions of plasma electrons with beam ions produce 4686Å optical photons that are observed using standard optical techniques. The beam time-of-flight between two nearby axial locations is determined by measuring the modulation phase shift of the photon signal between the two locations and the electrostatic potential is determined directly from the time-of-flight. The limitations imposed by incomplete beam penetration, photon counting statistics, and beam dispersion are examined. We obtain estimates for the uncertainty in the potential measurement at various locations on TMX-U and MFTF-B.

I. Introduction.

The present technique for measuring electrostatic potentials in tandem mirrors consists of a singly charged ion heavy ion (~200 amu) beam injected transverse to the magnetic field, and detectors which measure the charge states and energies of exiting ions[1]. The injected beam arcs through the plasma in a Larmor orbit with some chance of ionization as it moves along this path. From the energies and exit locations of the doubly charged beam ions, the potential inside the plasma can be inferred. This technique has been used successfully on TMX-U, but nevertheless suffers from several difficulties. One problem is that in magnetic field geometries which do not have cylindrical symmetry (e. g. quadrupole end plugs), the trajectories become very complicated, and it is doubtful whether the data can be correctly unfolded in these cases. The technique also suffers from an unfavorable scaling law. In order for the beam to penetrate the plasma and exit to reach the detectors, it can be shown that the beam energy scales as the square of the magnetic field times the chamber radius ($E \propto B^2a^2$). For a machine like MFTF-B, one finds that ion beams of several MeV are required. To obtain adequate signal, beam currents of several mA must be provided. This

combination of energy and current presents a formidable technical barrier.

Several measurement techniques have been studied which circumvent the problems of the heavy ion beam probe. An electron beam time-of-flight experiment, for example, was performed on the Multiple Mirror Experiment (MMX)[2]. A potential barrier in a single mirror cell was produced by short pulse ECRH heating. The formation and decay of a -40 V barrier was observed on 5 μsec timescales. A disadvantage of this technique, however, was that a current probe was physically inserted into the plasma to intercept the beam. Some methods for remotely detecting the electron beam are described in Ref. [2], but large background noise signals are present in those methods. The present report extends the time-of-flight concept to a He^+ beam measurement for which the background noise signal can be reduced to very low levels. The technique is indicated schematically in Figure 1. A density-modulated He^+ beam is injected axially along the central axial field line of a tandem mirror machine. Since the source density is modulated, the number of beam ions in the detection volume is modulated.

$$N_D(t) = N_{ave} + N_{peak} \sin(\omega t + \phi) \tag{1}$$

Optical photons produced by collisions with plasma electrons allow us to monitor the phase of the modulated beam. We relate the beam phase to the electrostatic potential as follows:

$$\phi(z) = \int_0^z \frac{\omega}{v(z')}\, dz' = \omega\sqrt{\frac{M}{2e}} \int_0^z [-V(z')]^{-1/2}\, dz', \tag{2}$$

where ω is the modulation frequency, and the beam velocity $v(z)$ varies with z due to variations in the electrostatic potential. Here the potential $V(z)$ is referenced to that of the He-discharge in the ion source. Differentiating (2) with respect to z, and solving for the potential we have

$$V(z) = -\frac{M\omega^2}{2e} [\phi'(z)]^{-2} \tag{3}$$

In this report we address various mechanisms which might destroy the beam and/or its information content, and we assess the sensitivity of the measurement.

II. Beam penetration – atomic processes.

There are a number of atomic processes which contribute to loss of beam. First we consider electron-impact ionization of beam ions.

$$He^+ + e^- \quad \rightarrow \quad He^{++} + 2e^-$$

The cross section for this process has been measured by Peart *et al.* [3], and these results are reproduced in Fig. 2. At high energies the cross section scales like $1/E$, as expected from the classical Thomson formula. We use this scaling to obtain approximate analytical estimates for the beam penetration. We calculate the number of excitations per second:

$$n < \sigma v >= \int_{v_{min}}^{\infty} \sigma(v) v f(v)\, d^3v$$

Taking $\sigma(v) = \beta/v^2$ and using a Maxwellian distribution we have

$$n < \sigma v >= n\beta \sqrt{\frac{2m}{\pi e T_e}} \exp\left(-E_{min}/eT_e\right)$$

where $E_{min} = 54\,\text{eV}$, the ionization energy for He^+. We estimate from Ref. [3] that $\beta \simeq 10.5\,\text{cm}^4/\text{sec}^2$. For TMX-U we assume a 10 keV beam with 500 eV electrons at 5×10^{12} cm^{-3} to estimate that

$$n < \sigma v >= 4 \times 10^4 \text{ sec}^{-1}$$

and the penetration distance (e-folding distance)

$$\lambda = \frac{v_b}{n < \sigma v >} \simeq 18\,\text{m}.$$

This value is to be compared with an overall length for TMX-U of ~20 m. The potential variations of interest (in the end plug) take place over a distance of ~5 m. For MFTF-B we take a 60 keV beam with 6 keV electrons at $10^{13}\,\text{cm}^{-3}$ to estimate $\lambda \simeq 65\,\text{m}$, which is to be compared with an overall machine length of ~40 m, and an end-plug length of ~10 m. The situation is more favorable in MFTF-B because of the higher electron temperatures and because higher beam energy is assumed in order to cross the 50 keV ion-confining potential.

In MFTF-B, however, charge transfer with H^+ can become important since there is a class of very hot ions expected in the center cell.

$$He^+ + H^+ \quad \rightarrow \quad He^{++} + \cdots$$

The reaction products include neutral hydrogen or H^+ and an electron. The total cross-section for this process has been measured[4], and these results are reproduced in Fig. 3. The cross-section peaks at 50 keV, which happens to be the ion temperature in the center cell. For a worst case estimate we take a delta-function ion distribution at 50 keV energy and 10^{13} cm^{-3} density to obtain $\lambda \simeq 27$ m.

In a fully ionized plasma we conclude that in both machines we expect complete penetration of the beam through the end plugs, but only partial penetration of the entire device.

The capture of electrons from neutral hydrogen may also be an important process:

$$He^+ + H \quad \rightarrow \quad He + H^+$$

This cross section is very difficult to measure (it requires a crossed beam experiment), and a literature search has failed to turn up any data. We expect the process to be the most significant beam interaction with neutrals, however, since the process is energetically favorable, and because the production of Franck-Condon neutrals in the halo plasma creates some H atoms energetic enough to penetrate into the plasma core. If we assume that the neutrals are cold, and that the cross section for the process is $20\pi a_0^2$ we have

$$\lambda = \frac{1}{20 n \pi a_0^2}$$

Requiring a penetration distance of 10 m, we obtain a density limit of $\sim 10^{12}$ cm^{-3} neutrals, which we expect to be much larger than the actual neutral density in the case of MFTF-B.

III. Beam penetration – plasma processes.

Dynamical friction exerted by the plasma on the beam ions slows the beam, and this effect cannot be distinguished from beam slowing due to an increase

in the plasma potential. For a Maxwellian distribution of field particles α

$$f_\alpha(v) = \frac{n_\alpha l_\alpha^2}{\pi^{3/2}} \exp\left(-l_\alpha^2 v^2\right) \tag{4}$$

where

$$l_\alpha^2 = m_\alpha / 2kT \tag{5}$$

The change in velocity per unit time for a particle of mass M, charge q, and velocity v_b is given by[5] (SI units)

$$\langle \Delta v_\parallel \rangle = -A_D l_\alpha^2 \left(1 + \frac{M}{m_\alpha}\right) G\left(l_\alpha v_b\right) \tag{6}$$

where $G(x)$ is the Chandrasekhar function

$$G(x) = \frac{\phi(x) - x\phi'(x)}{2x^2}, \tag{7}$$

$\phi(x)$ is the error function

$$\phi(x) = \frac{2}{\sqrt{\pi}} \int_0^x \exp\left(-y^2\right)\, dy \tag{8}$$

and A_D is the diffusion constant

$$A_D = \frac{q^2 q_\alpha^2 n_\alpha \ln \Lambda}{2\pi \epsilon_0^2 M^2}. \tag{9}$$

We consider a 10 keV He^+ beam in a 500 eV plasma at 5×10^{12} cm^{-3}. Over a distance of 20 m we find the energy loss due to protons to be

$$\Delta E \simeq M \langle \Delta v_\parallel \rangle \Delta z = 9.6\,\mathrm{eV} \tag{10}$$

while that due to electrons is even smaller ($\simeq 1.5\,$eV). The scaling is as follows:

$$\Delta E \propto n_\alpha G(l_\alpha v)/T_\alpha \tag{11}$$

Note that worst case occurs for $l_\alpha v_b = 1$, since $G_{max} = G(1) \simeq .214$. We conclude that dynamical friction is not a major difficulty.

A second plasma effect which could affect beam penetration is beam-plasma instabilities. These instabilities could convert beam particle energy

into wave energy in the plasma, or they could destroy the modulation coherence of the beam. We note at the outset of this analysis that the use of He^+ assures that the cyclotron frequency (eB/mc) of the beam ions is different from either plasma electrons or ions. Also the plasma frequency ($4\pi ne^2/M$) of the beam will be much less than that of either the electrons or the ions in the plasma. Briggs[6] has studied the problem of electron beam instabilities in great detail, and here we adapt those results to the He^+ beam. Let us first consider the case of longitudinal waves in an infinite unmagnetized homogeneous plasma with cold ions and warm electrons. The longitudinal dielectric function for the plasma is given by

$$K_{\|} = 1 - \frac{\omega_{pi}^2}{\omega^2} - \omega_{pe}^2 \int \frac{f_e(v_z)\, dv_z}{(\omega - kv_z)^2} \tag{12}$$

Now since the beam is weak (ω_{pb} is small), we expect the dispersion relation to be significantly modified only in the resonance region ($\omega = kv_b$). Taking a flat distribution for f_e we obtain the dispersion relation

$$1 = \frac{\omega_{pi}^2}{\omega^2} + \frac{\omega_{pe}^2}{\omega^2 - k^2 V_{Te}^2}. \tag{13}$$

This dispersion relation is plotted in Fig. (4). For reasonable parameters $v_b \ll V_{Te}$ and $v_b > V_{Te}\sqrt{m/M}$ (or equivalently, $E_{beam} > 2T_e$), so that the $\omega = kv_b$ curve does not cross the dispersion curves for the unperturbed plasma and there is no reactive-medium instability.

We must look at the imaginary part of the Landau integral in order to find the growth rate. The flat distribution function does not exhibit Landau damping, so we must use a more sophisticated model for the electron distribution function. We may approximate the Landau integral for the Maxwellian case in which $V_{Te} \gg v_b$.

$$I \doteq \omega_{pe}^2 \int \frac{f_e(v_z)\, dv_z}{(\omega - kv_z)^2} \simeq -\frac{\omega_{pe}^2}{k^2 V_{Te}^2}\left[1 - j\sqrt{\frac{\pi}{2}}\left(\frac{\omega}{kV_{Te}}\right)\right] \tag{14}$$

The dispersion relation in this case is given by

$$K_{\|} = \frac{\omega_{pb}^2}{(\omega - kv_b)^2} \tag{15}$$

where $K_\parallel$ is the longitudinal dielectric constant in the absence of the beam. Expanding about the point $\omega = kv_b$ we have

$$\frac{\beta_{bp}^2}{(\delta k)^2} = K_\parallel(\omega = kv_b) + \delta k \left(\frac{\partial K_\parallel}{\partial k}\right)_{\omega = kv_b} \tag{16}$$

Neglecting the last term on the right we have

$$(\delta k)^2 = \beta_{pb}^2 \frac{\omega^2/\omega_{pe}^2}{(\omega^2/\omega_{pe}^2) - (m/M) + (v_b/V_{Te})^2 \left[1 - j\sqrt{\frac{\pi}{2}}\,(v_b/V_{Te})\right]} \tag{17}$$

By differentiating with respect to ω we find that the maximum growth rate occurs at the frequency

$$\omega = \frac{\omega_{pe}}{\sqrt{2}} \frac{v_b}{v_{Te}} \tag{18}$$

For a 10kV, 1A beam of He^+ in a 500 eV plasma, with a beam radius of 3.5 cm we find have $\omega_{pb} = 3.2 \times 10^7$ rad/sec and the maximum growth rate is given by

$$\mathrm{Im}(\delta k) = .82\,\mathrm{m}^{-1}$$

This growth rate is substantial. However, $\mathrm{Re}(k)$ at the frequency given by (18) corresponds approximately to the Debye wavenumber, and it is not clear that this growth rate is meaningful. Furthermore, if we examine the growth rate at the beam modulation frequency (~ 5 MHz), we find

$$\mathrm{Re}(k) = .45\mathrm{m}^{-1} \qquad \mathrm{Im}(\delta k) = .008\,\mathrm{m}^{-1},$$

which implies a fairly small growth rate.

Further studies of beam-plasma effects will be undertaken which more closely model the real physical situation. The effects of finite beam transverse dimension and finite beam temperature will, for example, be studied.

IV. Excitation process.

Collisions of plasma electrons with beam ions produce $n = 4$ excited states of He^+, which emit a 4686Å optical photon upon relaxing to the $n = 3$

level. We are interested in the processes of excitation, subsequent mixing of l states, and photon emission to the $n = 3$ level.

First we consider the electron-impact excitation process.

$$He^+(1s) + e^- \quad \rightarrow \quad He^+(4l) + e^-$$

The cross sections for optically-allowed transitions ($\Delta l = 1$) scale as $\log E/E$ at energies much greater than threshold (51 eV), whereas electric dipole-forbidden cross sections scale as $1/E$. We have calculated all four cross sections in the Born approximation (Fig. 5). These results are in exact agreement with the Born approximation results given by Felden[7] for the $1s \rightarrow 4s$ and $1s \rightarrow 4p$ transitions. Here we have extended the calculation to include $1s \rightarrow 4d$ and $1s \rightarrow 4f$ cross sections. A more accurate approximation has been used to study the $1s \rightarrow 4s$ transition in Ref. [8], and those results are included for comparison. Near the peak, the values predicted by the Born approximation are typically twice the actual cross sections. Because of this over-estimation, the cross sections used in our uncertainty estimates are scaled as follows:

$$\sigma = \sigma_{Born}\,[.5 + .3107 \ln(E/E_T)] \qquad E \leq 5E_T$$

$$\sigma = \sigma_{Born} \qquad E > 5E_T$$

where E_T is the ionization threshold (51 eV). These two expressions give identical results at $5E_T$.

Now we consider the l-mixing processes which may mix l-states prior to radiative recombination.

$$\begin{aligned} He^+(4l) + e^- \quad &\rightarrow \quad He^+(4l') + e^- \\ He^+(4l) + H^+ \quad &\rightarrow \quad He^+(4l') + H^+ \end{aligned}$$

If the plasma density is very high, collisions of protons and electrons with the excited state will induce l-mixing of the excited state, and a statistical distribution of states will evolve. Thus the population of each l state is weighted by $(2l+1)$, regardless of its individual excitation cross section. In a very tenuous plasma, however, the radiative lifetime becomes short compared to the mixing lifetime, and the different l states do not mix. Olson has calculated the cross sections for these process using a Monte Carlo classical

Density (cm^{-3})	Mixing
$< 5 \times 10^{12}$	None
$5 \times 10^{12} - 5 \times 10^{14}$	$4s \rightarrow 4p$
$5 \times 10^{14} - 5 \times 10^{15}$	Complicated ($\tau_{rad} \sim \tau_{mix}$)
$> 5 \times 10^{15}$	Complete mixing

Table 1: Density criteria for l-mixing of $4l$ states of He^+.

trajectory method[9], and these results are duplicated in Fig. 6. The scaling for these cross sections is that $\sigma_{mix}v$ ~constant. Comparing τ_{rad} with τ_{mix} we may infer the approximate results of Table 1. For typical TMX-U densities there is no mixing, and for projected MFTF-B densities the $4s$ state will be collisionally converted to the $4p$ state before radiative decay.

Finally, we examine the photon emission process.

$$He^+(4l) \quad \rightarrow \quad He^+(3l') + h\nu\,(4686\text{Å})$$

The branching ratios of Table 2 were calculated using transition rates given in [10]. These branching ratios are multiplied by the excitation rates $n\langle\sigma v\rangle$ to obtain the production rate for 4686Å emission. The photon production rate for a single He^+ ion is then given by

$$\gamma = \sum_l B_l n \langle\sigma(1s \rightarrow 4l)v\rangle \sec^{-1} \tag{19}$$

Due to l-mixing, $B_0 \rightarrow B_1$ for $n \gtrsim 5 \times 10^{12}$ cm^{-3}. The total measured count rate is obtained by multiplying (19) by the number of beam ions in the detection volume, the solid angle subtended by the detection optics, and the detector efficiency.

$$\gamma = L\frac{I}{ev_b}\frac{\Omega}{4\pi}\eta \sum_l B_l n \langle\sigma(1s \rightarrow 4l)v\rangle \sec^{-1} \tag{20}$$

where L is the length of the detection volume, Ω is the detector solid angle, and η is the detector efficiency.

Initial state	Total transition rate (10^8 sec)	Branching ratio (%) to $n = 3$ level
4s	.69	42
4p	13.0	4.1
4d	4.38	26
4f	2.19	100

Table 2: Branching ratios for relaxation of $4l$ states in He^+ to the $n = 3$ level.

V. Uncertainty in the measurement.

Photon counting statistics place a fundamental limitation on the sensitivity of a phase measurement. We address the problem of extracting phase information from a digitally-recorded photon signal. Suppose the true signal consists of

$$S_j = S_{A0} + S_{P0} \sin(\omega t_j + \phi_0) \tag{21}$$

photons/subinterval j. If the noise signal is F_j, then we observe a total signal

$$P_j = S_j + F_j \tag{22}$$

We now seek to minimize the error

$$e = \sum_{j=1}^{J} \left[S_A + S_P \sin\left(\omega t_j + \overline{\phi}\right) - P_j \right]^2 \tag{23}$$

by setting $\partial e/\partial S_A = \partial e/\partial S_P = \partial e/\partial \overline{\phi} = 0$. This procedure results in the set of equations

$$\begin{aligned} S_A &= \tfrac{1}{J} \sum_{j=1}^{J} \left[P_j - S_P \sin\left(\omega t_j + \overline{\phi}\right) \right] \\ S_P &= \tfrac{2}{J} \sum_{j=1}^{J} P_j \sin\left(\omega t_j + \overline{\phi}\right) \\ &\sum_{j=1}^{J} P_j \cos\left(\omega t_j + \overline{\phi}\right) = 0 \end{aligned} \tag{24}$$

The uncertainty in the mean phase $\overline{\phi}$ can be found by inserting (21) and (22) into the last of Eqs. (24) to obtain

$$\sum_{j=1}^{J} S_P \sin(\omega t_j + \phi_0) \cos\left(\omega t_j + \overline{\phi}\right) + \sum_{j=1}^{J} F_j \cos\left(\omega t_j + \overline{\phi}\right) = 0. \tag{25}$$

Now we assume that $\overline{\phi}$ is close to ϕ_0

$$\overline{\phi} = \phi_0 + \Delta\phi\,; \qquad \Delta\phi \ll 2\pi, \tag{26}$$

$S_A \approx S_{A0}$, and $S_P \approx S_{P0}$, so that (25) becomes

$$S_P \Delta\phi(J/2) = \sum_{j=1}^{J} F_j^{(k)} \cos\left(\omega t_j + \overline{\phi}\right). \tag{27}$$

The noise is proportional to the square root of the number of counts

$$F_j^{(k)} = U_j^{(k)} \sqrt{S_A + S_P \sin(\omega t_j + \phi_0)} \tag{28}$$

where k is an ensemble designator over which we will average. $U_j^{(k)}$ represents the Gaussian-distributed random variables such that

$$\frac{1}{k}\sum_k U_j^{(k)} = 0 \quad \text{and} \quad \frac{1}{k}\sum_k U_i^{(k)} U_j^{(k)} = \delta_{ij}. \tag{29}$$

Substituting (28) into (27) we find

$$\overline{(\Delta\phi)^2} = \frac{2}{J}\frac{S_A}{S_P^2}. \tag{30}$$

Now we use $JS_A = N_T$, the total number of photons collected, to arrive at the rms uncertainty in the phase measurement:

$$\Delta\phi_{rms} = \frac{S_A}{S_P}\sqrt{\frac{2}{N_T}}. \tag{31}$$

Note that $S_A \geq S_P$, and that equality gives the most favorable uncertainty estimate. This result implies that a greater fractional beam modulation

improves the measurement. Also the uncertainty improves as the number of photons collected increases, which is as expected.

Several sources of background count rate (S_A) may be readily identified:

- He leakage from superconducting magnets (in MFTF-B)
- Neutrals ejected from He^+ source
- Incomplete beam modulation
- Beam dispersion due to finite beam temperature
- Impurity radiation (e. g. N III at 4640Å)
- Bremsstrahlung

The beam dispersion effect will be addressed in greater detail later in this report. Other sources of noise could be evaluated empirically.

We now seek a relationship between the uncertainty in the phase measurement and the uncertainty in the electrostatic potential.

In order to use (3) to obtain the potential we estimate ϕ' from the phase at two axial locations

$$\phi' = \frac{\phi_2 - \phi_1}{L} \tag{32}$$

where L is the axial separation. We note that ϕ' has the mean

$$\overline{\phi'} = \frac{\overline{\phi}_2 - \overline{\phi}_1}{L} \tag{33}$$

and the rms deviation

$$\Delta\phi'_{rms} = \frac{\sqrt{2}\Delta\phi_{rms}}{L}. \tag{34}$$

From (3) we see that V has the mean

$$\overline{V} = \frac{M\omega^2}{2e\left(\overline{\phi'}\right)^2} \tag{35}$$

and the rms deviation

$$\Delta V_{rms} = \frac{M\omega^2}{e\left(\overline{\phi'}\right)^3}\Delta\phi'_{rms} \tag{36}$$

Inserting (34) and (35) into (36) we obtain

$$\Delta V_{rms} = \frac{4}{\omega}\sqrt{\frac{e}{M}}\,\overline{V}^{3/2}\,\frac{\Delta\phi_{rms}}{L} \tag{37}$$

VI. Loss of coherence due to finite beam temperature.

Finite beam temperature gives rise to a loss of coherence as the beam propagates down the machine. The parallel temperature ($T_\parallel$) gives rise to dispersion of the density oscillations as faster beam ions outrun slower ones. The perpendicular temperature ($T_\perp$) gives rise to a similar effect as particles with higher magnetic moment see a larger mirroring force than those with smaller magnetic moment.

These finite beam temperature effects are included in the numerical model described in Section VII.. In the present section we present an analytical calculation for the beam dispersion in the mirror geometry of Fig. 7. First we note that the effective parallel temperature of the beam is reduced by the acceleration process in the ion source.

$$E_\parallel = e\left(T_\parallel + V_b\right) = \tfrac{1}{2} M v_{\parallel 0}^2 \tag{38}$$

Solving for $v_{\parallel 0}$ and taking $T_\parallel \ll V_b$ we have

$$v_{\parallel 0} \simeq v_b \left[1 + \frac{T_\parallel}{2V_b}\right] \tag{39}$$

The spread in velocity is given by

$$\Delta v_{\parallel 0} \simeq \frac{v_b T_\parallel}{2V_b} = \sqrt{\frac{eT_{eff}}{M}} \tag{40}$$

where

$$T_{eff} = T_\parallel \left[\frac{T_\parallel}{2V_b}\right].$$

The term in brackets corresponds to an effective reduction in the parallel temperature due to source acceleration.

Now taking the mirroring force as

$$F = -\mu \nabla_\parallel B \tag{41}$$

we obtain an expression for the longitudinal dispersion:

$$\Delta z = \left\{ \left[\frac{\Delta v_{\|0}}{v_b} (l_0 + l_M + l_1) \right]^2 + \left[\frac{v_{\perp 0}^2 B_1}{2 v_b^2 B_0} \left(\frac{l_M}{2} + l_1 \right) \right]^2 \right\}^{1/2} . \qquad (42)$$

The first three terms are due to the finite parallel temperature, and the last two are due to the mirroring force. The mirroring force is the dominant source of dispersion for $T_{\|} \sim T_{\perp}$ and $B_1 \gg B_0$. The beam dispersion effect on the measurement is small as long as the spread Δz is much smaller than a modulation wavelength. Taking the parameters

$$l_0 = 5\,\mathrm{m} \qquad l_M = 2\,\mathrm{m} \qquad l_1 = 2\,\mathrm{m}$$

$$B_0 = .015\,\mathrm{T} \qquad B_1 = 2\,\mathrm{T}$$

$$V_b = 10\,\mathrm{keV} \qquad T_{\|} = 3\,\mathrm{eV} \qquad T_{\perp} = 1\,\mathrm{eV}$$

we find that $\Delta z \simeq 1.0\,\mathrm{cm}$. The observation wavelength is typically $\sim$5 cm.

Both this analytical result and the simulation results of Section VII. assume conservation of the magnetic moment, an assumption which is valid provided that

$$\epsilon \equiv \frac{1}{\omega^2} \frac{d\omega}{dt} \ll 1, \qquad (43)$$

or

$$\frac{v_b}{\omega_{ci}} \ll L_B \qquad (44)$$

where L_B is the scale length of magnetic field variations. This condition is satisfied everywhere but near the end wall, where the magnetic fields become very small, and the corresponding gyrofrequency becomes small. To study this region requires a different approximation; future studies will consider the question of beam dispersion under the paraxial ray approximation.

VII. Potential uncertainty for TMX-U and MFTF-B.

A computer model has been developed which predicts the uncertainties for this measurement for typical TMX-U and MFTF-B configurations. The model takes the following input parameters:

- Beam characteristics
  - Energy
  - Beam current vs. time
  - Temperature ($T_\perp$ and $T_\parallel$)
- Machine configuration
  - Axial potential profile
  - Axial magnetic field profile
  - Electron distribution functions
- Observation parameters
  - Quantum efficiency of detector (η)
  - Desired spatial and temporal resolution
  - Solid angle of detector

The following effects are taken into account in the calculation:

- Loss of beam due to electron impact ionization
- Beam dispersion
- Excitation process
- Counting statistics

The code first calculates the number of beam ions in the detection volume vs. time. To compute this quantity, the unaccelerated distribution function is assumed to be of the form

$$f(t) = \alpha(t) \exp\left\{-Mv_\parallel^2/2eT_\parallel - Mv_\perp^2/2eT_\perp\right\}. \tag{45}$$

The normalization $\alpha(t)$ is fixed by a knowledge of the time variation of the source current:

$$I(t) = eA \int v_\parallel f(t)\, v_\perp dv_\perp dv_\parallel \tag{46}$$

where A is the area of the beam. The number of beam ions leaving the source with parallel velocity $v_\parallel \pm \Delta v_\parallel/2$ and perpendicular velocity $v_\perp \pm \Delta v_\perp/2$ is given by

$$\begin{aligned} s(t;\, v_\parallel, v_\perp) &= v_\parallel f(t)\, d^3v = v_\parallel f(t) \Delta v_\parallel\, v_\perp \Delta v_\perp \\ &= v_\perp v_\parallel \frac{M^2 I(t)}{e^3 T_\parallel T_\perp} \exp\left\{-M v_\parallel^2/2eT_\parallel - M v_\perp^2/2eT_\perp\right\} \Delta v_\parallel \Delta v_\perp \end{aligned} \tag{47}$$

The particles in this differential element of velocity space enter and exit the detection volumes at times which we will denote as t_1 and t_2, respectively. Their contribution to the number of particles in the detection volume is given by

$$N(t;\, v_\parallel, v_\perp) = \int_{t-t_2}^{t-t_1} s(t';\, v_\parallel, v_\perp)\, dt'. \tag{48}$$

Finally, we integrate this expression over velocity space to obtain the number of beam ions in the detection volume vs. time:

$$\begin{aligned} N_D(t) = \frac{M^2}{e^3 T_\parallel T_\perp} \int_0^\infty dv_\perp \int_0^\infty dv_\parallel v_\perp v_\parallel \\ \exp\left\{-M v_\parallel^2/2eT_\parallel - M v_\perp^2/2eT_\perp\right\} \int_{t-t_1}^{t-t_2} dt'\, I(t'). \end{aligned} \tag{49}$$

The delay times t_1 and t_2 depend on $v_\perp$ and $v_\parallel$ through the expression

$$t_{1,2} = \int_0^{z_{1,2}} \frac{dz}{v_\parallel(z)}, \tag{50}$$

where

$$v_\parallel^2(z) = \frac{2}{M}\left[E - \mu B(z) - e\Phi(z)\right].$$

The value of E is set by the expression

$$E = \tfrac{1}{2} M (v_\parallel^2 + v_\perp^2) + eV_{acc} + e\Phi(z=0),$$

where V_{acc} is the beam acceleration potential.

Finally, the value of N_D obtained from (49) is reduced by the fraction

$$f(z) = \exp\left\{-\int_0^z \frac{n(z')\langle\sigma v\rangle}{v_\parallel(z')}\, dz'\right\}$$

where σ is the cross section for electron impact ionization. The photon production is then computed using (20), and converted to an uncertainty in phase using (31). Finally, (37) is used to predict the uncertainty in potential. Fig. 8 gives the parameters used to obtain the uncertainty estimates of Fig. 9 for TMX-U, and Fig. 10 gives the MFTF-B parameters used to obtain the results given in Fig. 11. The uncertainty estimates appear quite favorable for both of these machines.

VIII. Conclusions.

A technique for measuring electrostatic potential variations in tandem mirrors has been proposed, and various difficulties which the measurement would face have been addressed. It appears that none of these difficulties preclude the success of the measurement. We have obtained uncertainty estimates which appear quite favorable for both the TMX-U and MFTF-B tandem mirror experiments. At this time three major questions remain to be studied. First, the beam-plasma instability problem requires further theoretical analysis. Second, the effects of magnetic field errors and non-adiabaticity of the beam ion trajectories must be studied. Finally, the beam technology assumed in this report is not highly developed, as few experiments require a high frequency, density-modulated ion beam. An experiment is planned on the Multiple Mirror Experiment at U. C. Berkeley which will address the feasibility of producing such a beam. Also the difficulites posed by magnetic field errors and beam-plasma instabilities will be investigated.

References

[1] Hornady, R. S., Coutts, G. W., Colborn, J. A., Heefner, J. W., and Nelson, D. H., Plasma Potential in the TMX-U Central Cell, Bull. Am. Phys. Soc., 26th Annual Meeting of the Division of Plasma Physics, Abstract #8S20, (1984).

[2] Lieberman, M. A., and Chang, C. P., Electron Beam Time-of-Flight Measurements of Plasma Potential in Tandem Mirrors, UCB Memorandum No. UCB/ERL M84/92 (1984).

[3] Peart, B., Walton, D. S., and Dolder, K. T., J. Phys. B, **2**, 1347-1352 (1969).

[4] Peart, B., Rinn, K., and Dolder, K., J. Phys. B, **16**, 1461-1469 (1983).

[5] Schmidt, G., **Physics of High Temperature Plasmas**, 2nd ed., Academic Press, (1979).

[6] Briggs, R. J., **Electron-Stream Interaction with Plasmas**,M. I. T. Press, (1964).

[7] Felden, M. M., and Felden, M. M., The Astrophys. J., **174**, 219-226 (1972).

[8] McDowell, M. R. C., Morgan, L. A., and Myerscough, V. P., J. Phys. B, **6**, 1435-1451 (1973).

[9] Olson, R. E., U. of Missouri, Fifth Topical Conference on Atomic Processes in High Temperature Plasmas, Paper #C-6, Feb. 25-28, 1985.

[10] Condon, E. U., and Shortley, G. H., **The Theory of Atomic Spectra**, Cambridge University Press (1979).

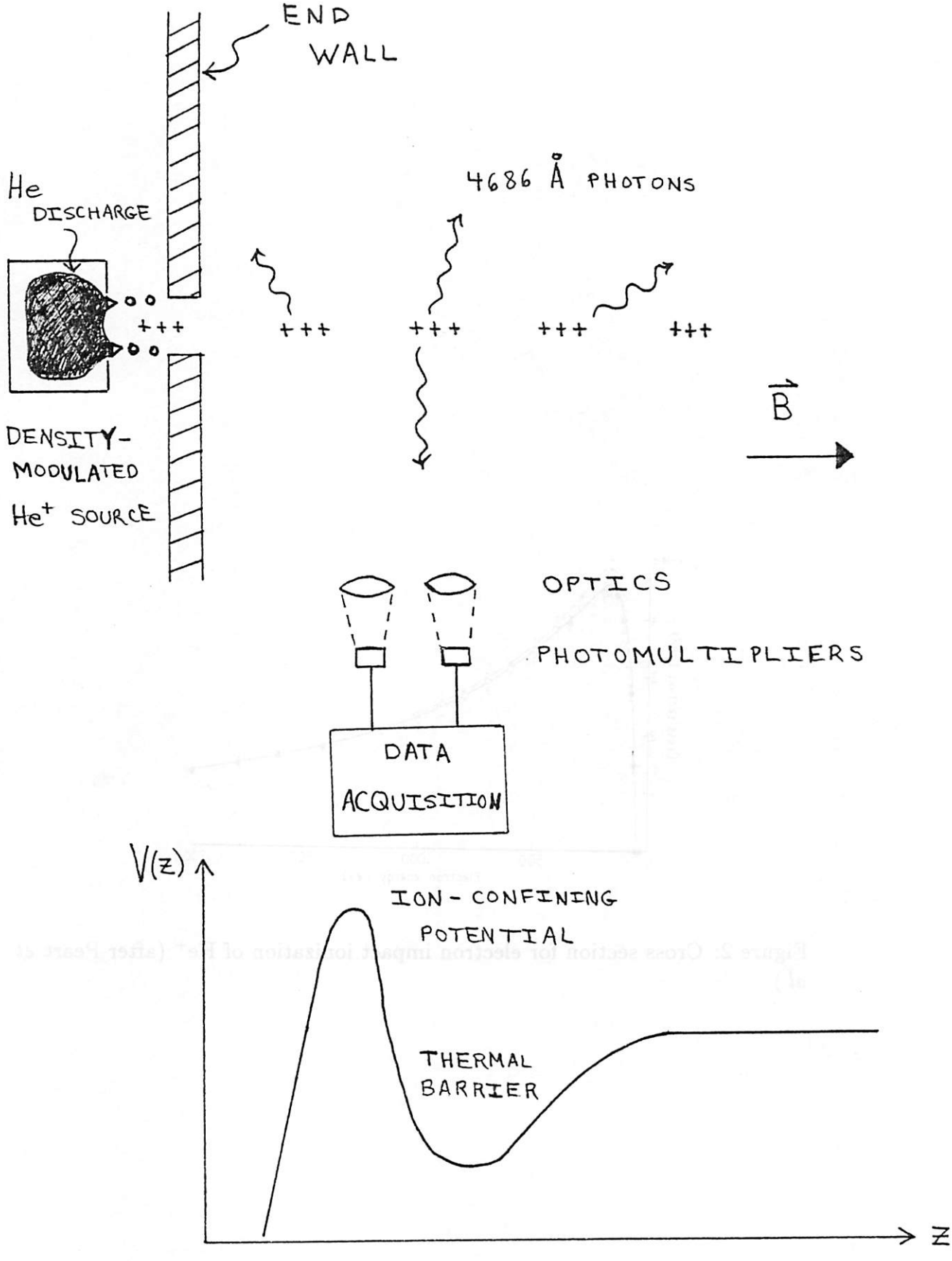

Figure 1: Principle of the measurement.

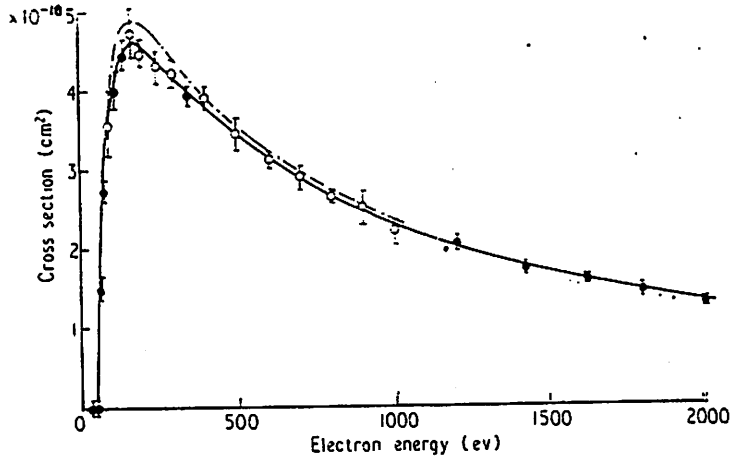

Figure 2: Cross section for electron impact ionization of He^+ (after Peart *et al.*).

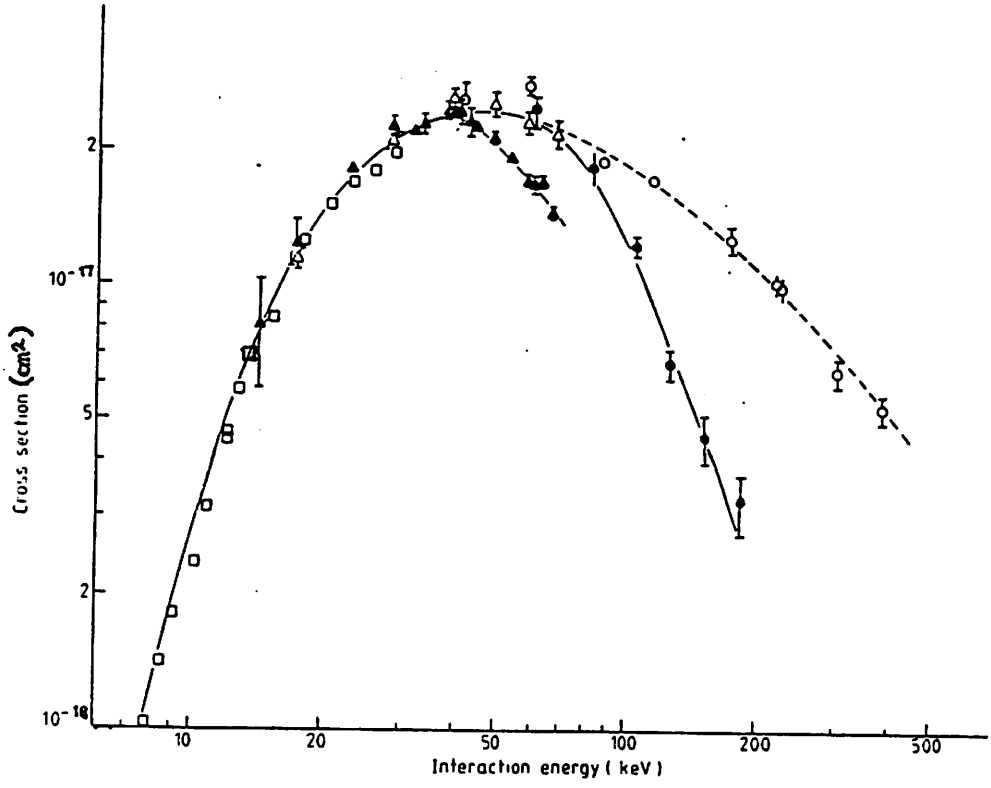

Figure 3: Cross section for production of He^{++} by collisions with protons (after Peart *et al.*).

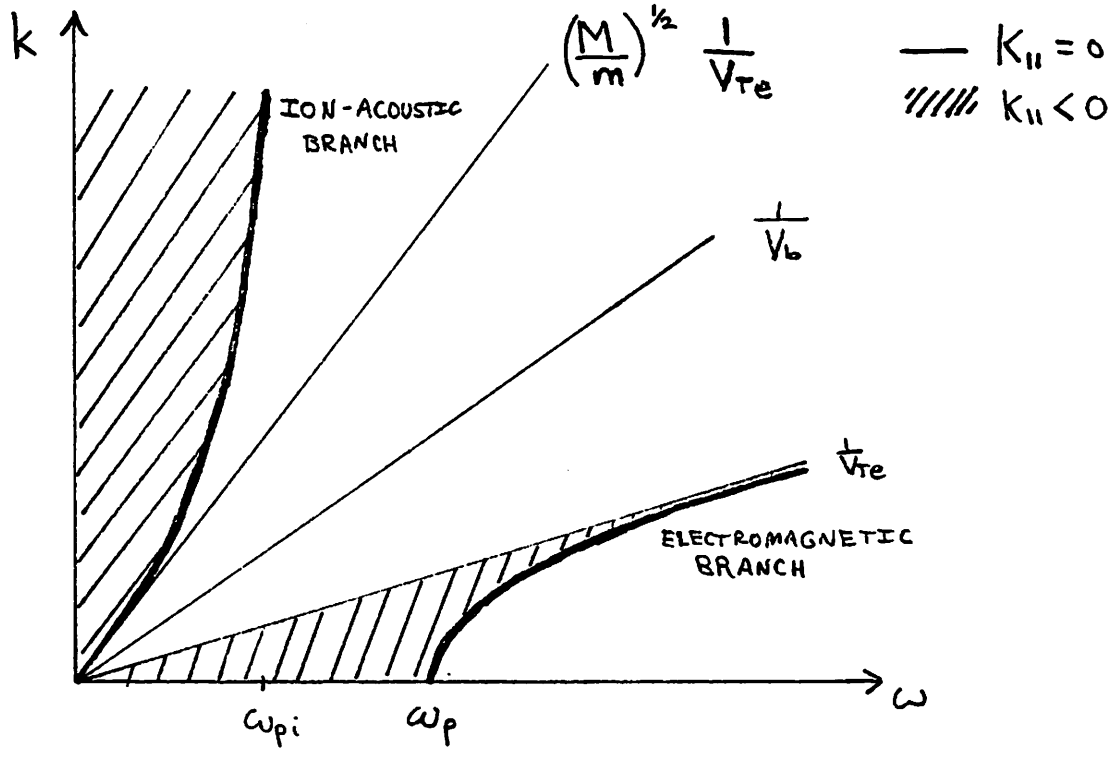

Figure 4: Dispersion relation for unmagnetized plasma with cold ions and warm electrons (flat distribution).

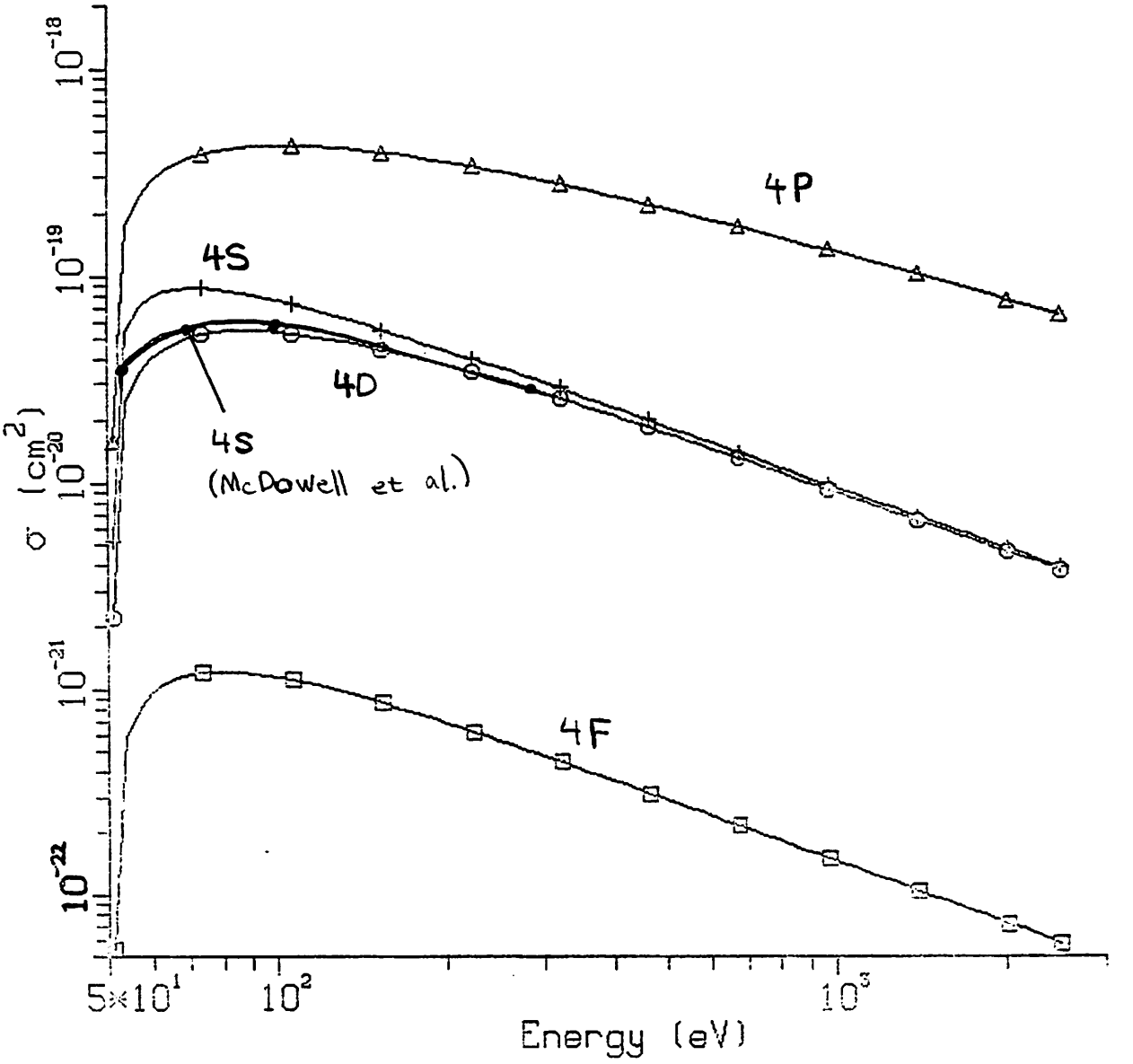

Figure 5: Electron impact excitation cross sections (Born approximation) for $1s \rightarrow 4l$ transitions in He^+.

$$He^+(4l) + e^- \rightarrow He^+(4l') + e^-$$

$$E(e^-) = 2\,\text{keV}$$

		Final states				
		4s	4p	4d	4f	k_{rad}
Initial states	4s	–	1.5(-5)	3.0(-8)	<3.0(-8)	6.9(7)
	4p	4.6(-6)	–	8.8(-6)	<3.0(-8)	1.3(9)
	4d	<3.0(-8)	6.1(-6)	–	6.0(-6)	4.4(8)
	4f	<3.0(-8)	<3.0(-8)	4.6(-6)	–	2.2(8)

$$He^+(4l) + H^+ \rightarrow He^+(4l') + H^+$$

$$E(H^+) = 50\,\text{keV}$$

		Final states				
		4s	4p	4d	4f	k_{rad}
Initial states	4s	–	1.1(-5)	8.4(-7)	7.4(-8)	6.9(7)
	4p	3.5(-6)	–	6.7(-6)	2.4(-7)	1.3(9)
	4d	1.3(-7)	3.8(-6)	–	4.6(-6)	4.4(8)
	4f	1.4(-8)	8.8(-8)	3.4(-6)	–	2.2(8)

Figure 6: Collisional l-mixing of He^+ $n = 4$ states. The tables give values for (σv) in cm^3/sec at the indicated energies (after Olson). Rates are obtained by multiplying by density. The last column gives the radiative rate in sec^{-1}.

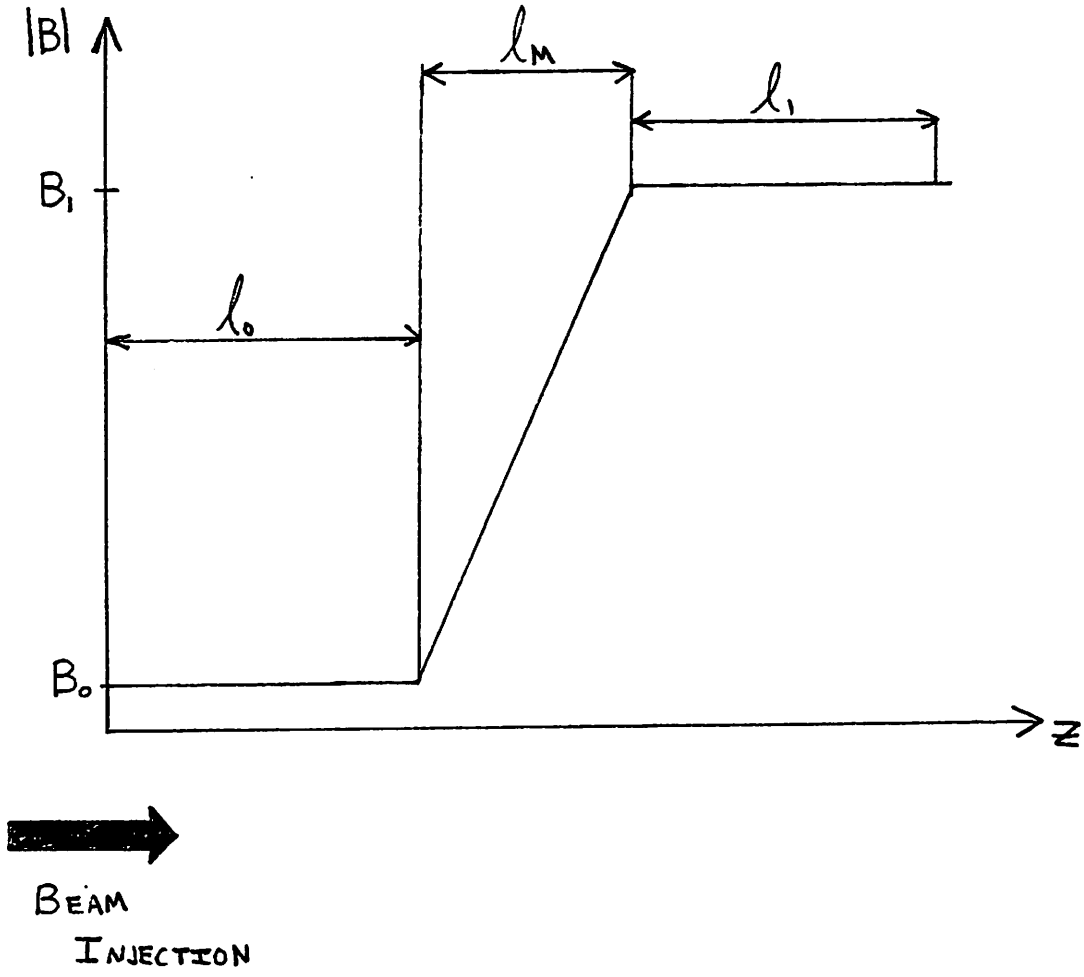

Figure 7: Mirror geometry for analytical beam dispersion estimate.

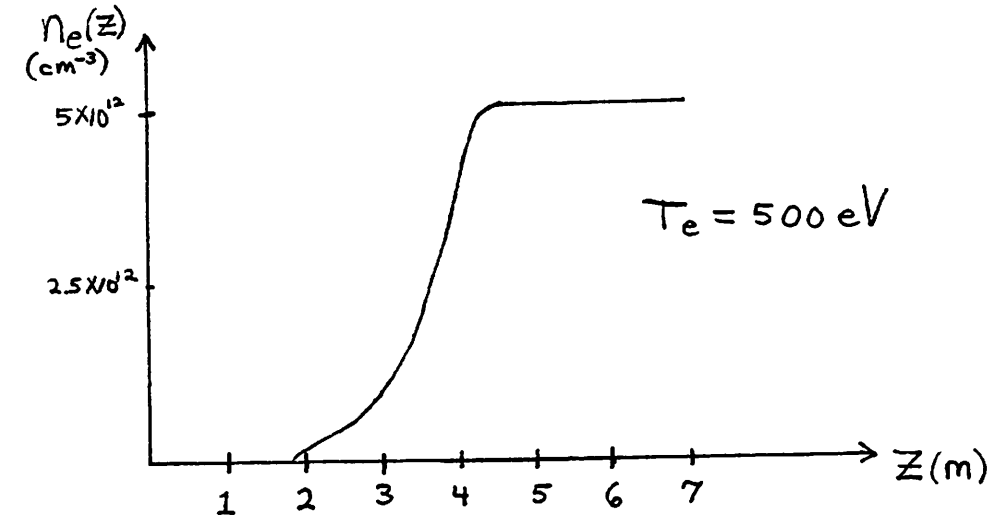

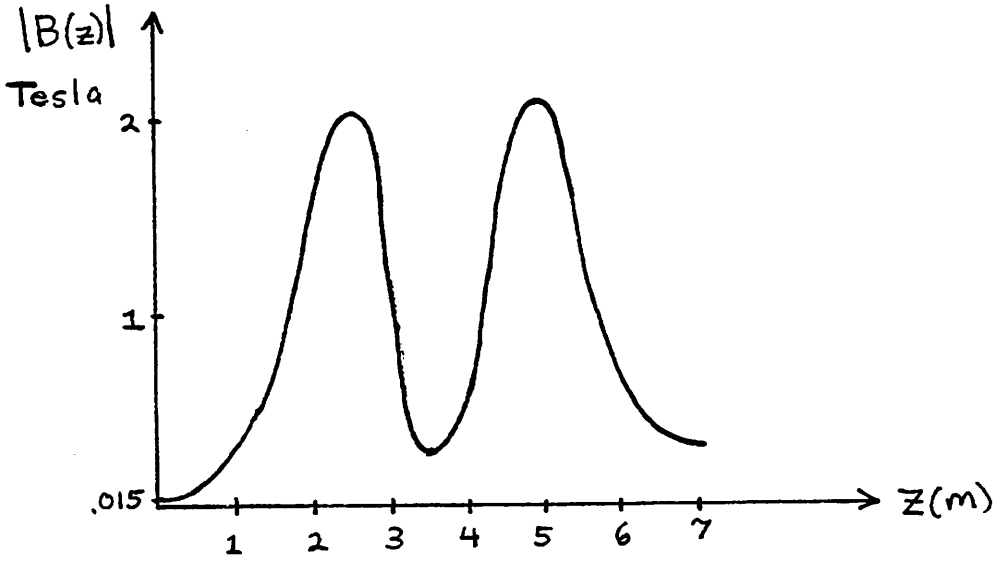

Beam characteristics:

50% modulation	$T_\perp = 3\,\text{eV}$	$T_\parallel = 10\,\text{eV}$
$E_{beam} = 10\,\text{keV}$	$f = 6.6\,\text{MHz}$	$I_{peak} = 1\,\text{A}$

Observation parameters:

$$\Omega = .002 \qquad \eta = .2 \qquad T_{ave} = 1\,\text{ms}$$

Mixing: NONE

Figure 8: Conditions for TMX-U uncertainty calculations of Fig. 9.

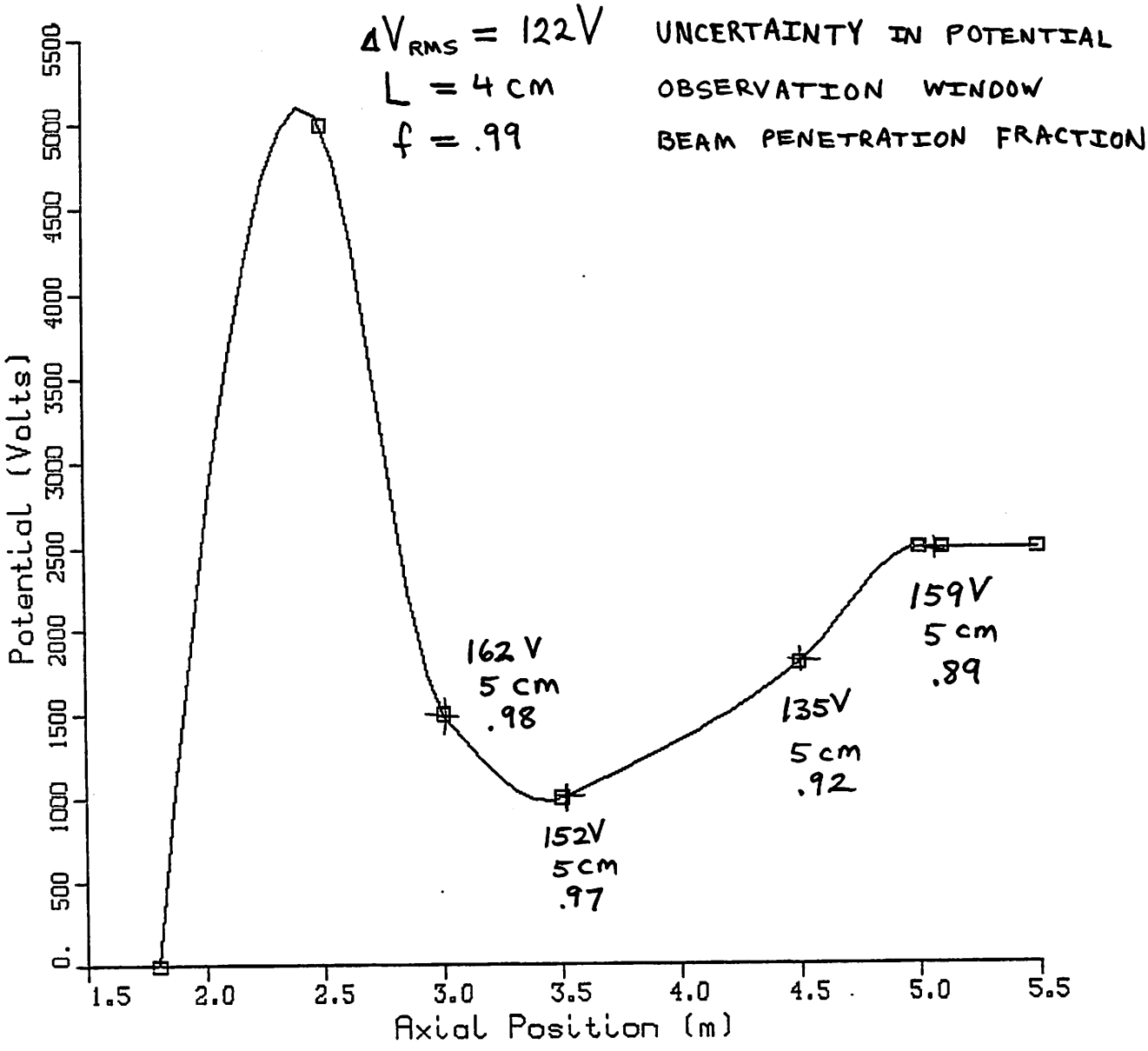

Figure 9: End plug potential of TMX-U. Uncertainty estimates for the potential (in volts) as measured by the He^+ beam time-of-flight diagnostic are indicated at various points of the profile.

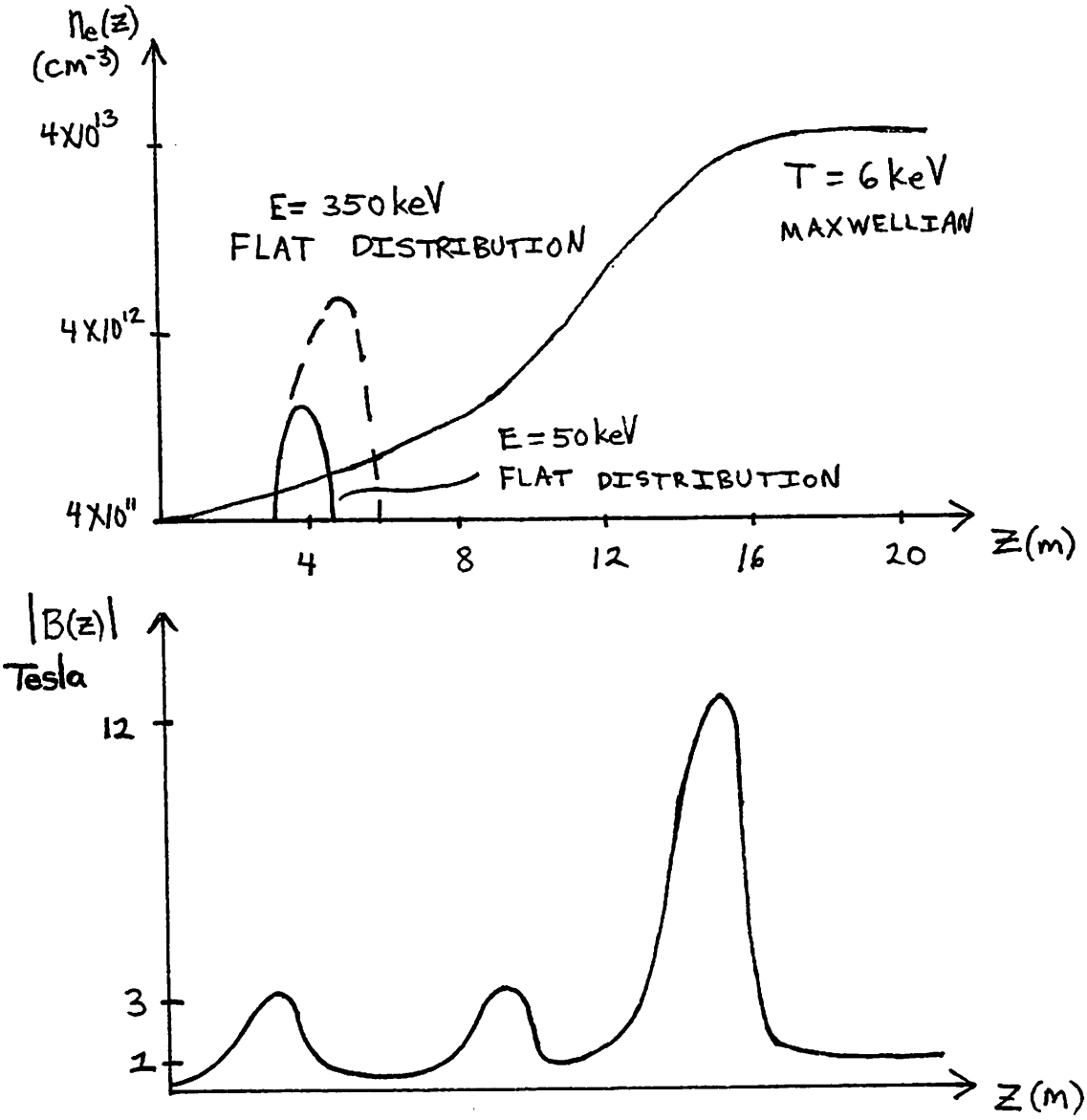

Beam characteristics:

50% modulation	$T_\perp = 3\,\text{eV}$	$T_\parallel = 10\,\text{eV}$
$E_{beam} = 60\,\text{keV}$	$f = 4.2\,\text{MHz}$	$I_{peak} = 2\,\text{A}$

Observation parameters:

$$\Omega = .0002 \qquad \eta = .2 \qquad T_{ave} = 5\,\text{ms}$$

Mixing: $B_0 \rightarrow B_1$

Figure 10: Conditions for MFTF-B uncertainty calculations of Fig. 11.

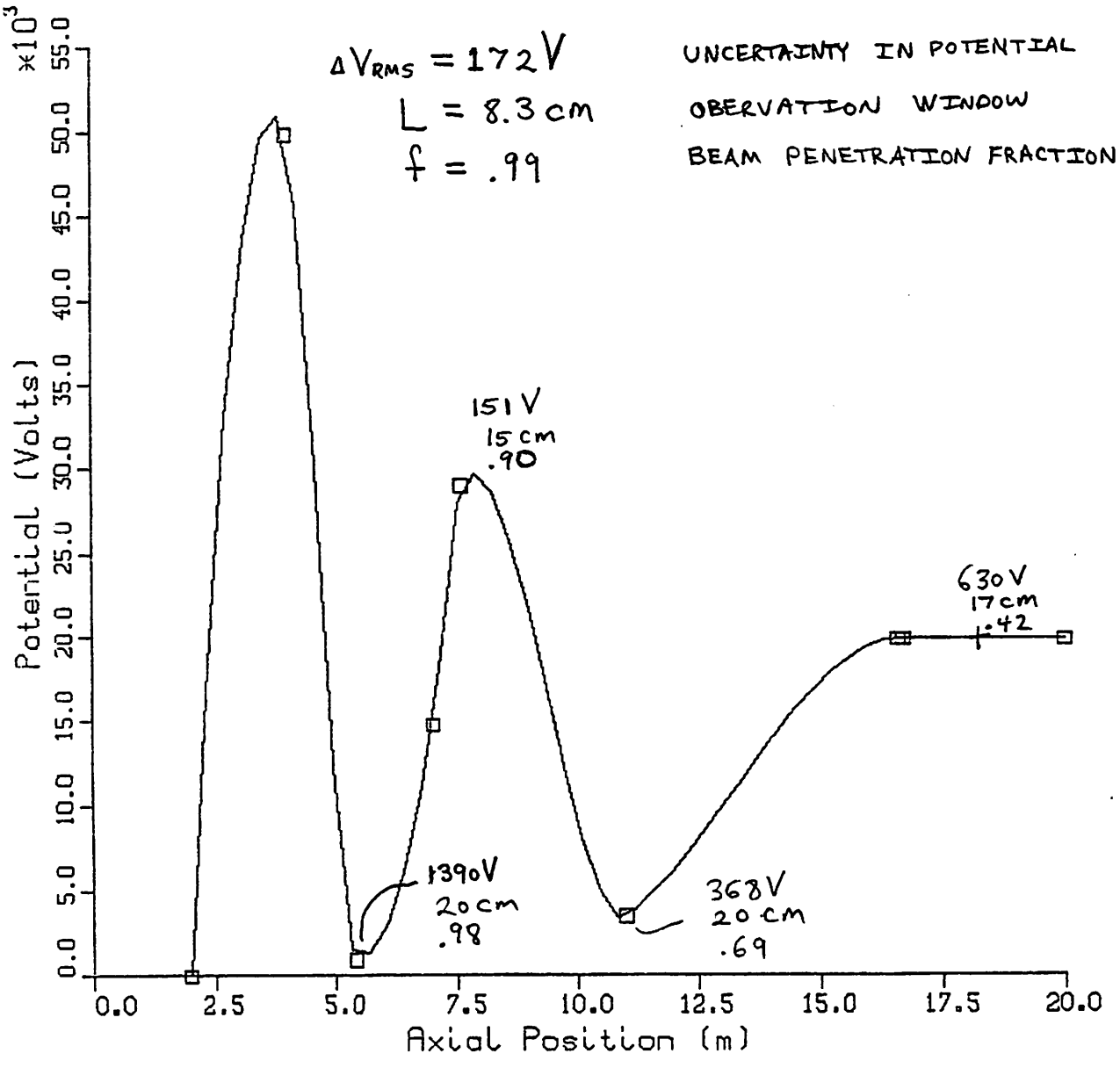

Figure 11: End plug potential of MFTF-B. Uncertainty estimates for the potential (in volts) are indicated at various points of the profile.